Target tracking control of a bionic mantis shrimp robot with closed-loop central pattern generators

Target tracking control of a bionic mantis shrimp robot with closed-loop central pattern generators

Gang Chen [a,b], Yidong Xu [a], Xin Yang [a], Huosheng Hu [b], Hao Cheng [c], Lvyuan Zhu [d], Jingjing Zhang [e], Jianwei Shi [e], Xinxue Chai [a]

[a] School of Mechanical Engineering, Zhejiang Sci-Tech University, Hangzhou 310018, China
[b] School of Computer Science and Electronic Engineering, University of Essex, Colchester CO4 3SQ, UK
[c] Zhejiang Institute of Industry and Information Technology, Hangzhou 310000, China
[d] Zhejiang Machinery Industry Federation, Hangzhou 310009, China
[e] Zhejiang CathayBot Technology Co., Ltd., Jinhua 321035, China

A B S T R A C T

To address the challenge of efficient underwater target tracking, this study focuses on the mantis shrimp as a biomimetic model. The research involves the design of a bionic mantis shrimp robot featuring a structure that supports multi-pleopod coupled movement. We propose a target tracking control system based on a bionic closed-loop central pattern generator (CPG). This system integrates CPG control, proportional integral derivative control, and fuzzy logic control. It aims to enable precise target tracking by dynamically adjusting the robot's motion in response to data from vision sensors. Extensive underwater experiments validate the effectiveness of this control system in both static and dynamic target tracking scenarios. The experiments demonstrate that the bionic mantis shrimp robot can perform multiangle turns and adjust its velocity flexibly in a confined space measuring 2 m × 1 m × 1 m. Notably, the robot can track targets at angles up to 130° relative to its initial motion direction. The minimum tracking turning radius achieved is 0.65 m, highlighting the potential for advanced target tracking and broader applications in underwater robotics.

1. Introduction

Target tracking by underwater robots is an emerging field in robotics technology. It enables robots to autonomously pursue objects submerged in aquatic environments, offering valuable assistance in tasks such as underwater target search, salvage operations, rescue missions, and tracking marine life. The primary challenges in current underwater target tracking technology revolve around underwater vision and robot motion control. Factors such as temperature, humidity, water flow, turbidity, noise, and other environmental variables can influence the accuracy of underwater target detection and tracking. Additionally, robot motion in water is susceptible to nonlinear disturbances, necessitating both robust motion performance and stability. Over millions of years of evolution, marine organisms have developed exceptional locomotion abilities, including high velocity, efficiency, and agility. The mantis shrimp stands out as a representative species with powerful forelimbs (Li et al., 2022), excellent swimming capabilities (Garayev and Murphy, 2021), and unique vision (Blair et al., 2021). Its flat body can flex freely, and its five pairs of flexible, soft pleopods provide strong propulsion (Chen et al., 2023a). This allows it to achieve rapid swimming and agile maneuvering in narrow underwater spaces, exhibiting remarkable maneuverability.

Drawing inspiration from nature, many bionic underwater robots have emerged (Yu et al., 2018). For example, Muralidharan et al. employed shape memory alloys to design bionic fish, demonstrating bidirectional shape memory effects (Muralidharan and Palani, 2021). Chen et al. proposed a bionic robotic manta ray utilizing an ionic polymer metal composite as an artificial muscle to mimic manta ray swimming behavior (Chen et al., 2012). Wang et al. introduced the concept of a shallow crab-like robot with a hybrid leg-paddle drive and designed its gait (Wang et al., 2017). Our research laboratory is also engaged in various bionic robotics studies, including intelligent control of beaver-like robots and neural network-based control of soft robot fish (Chen et al., 2022, 2023b, 2023c). The remarkable locomotion abilities of the mantis shrimp make it an ideal candidate for bionic inspiration in underwater robotics. Surprisingly, there has been no prior research on

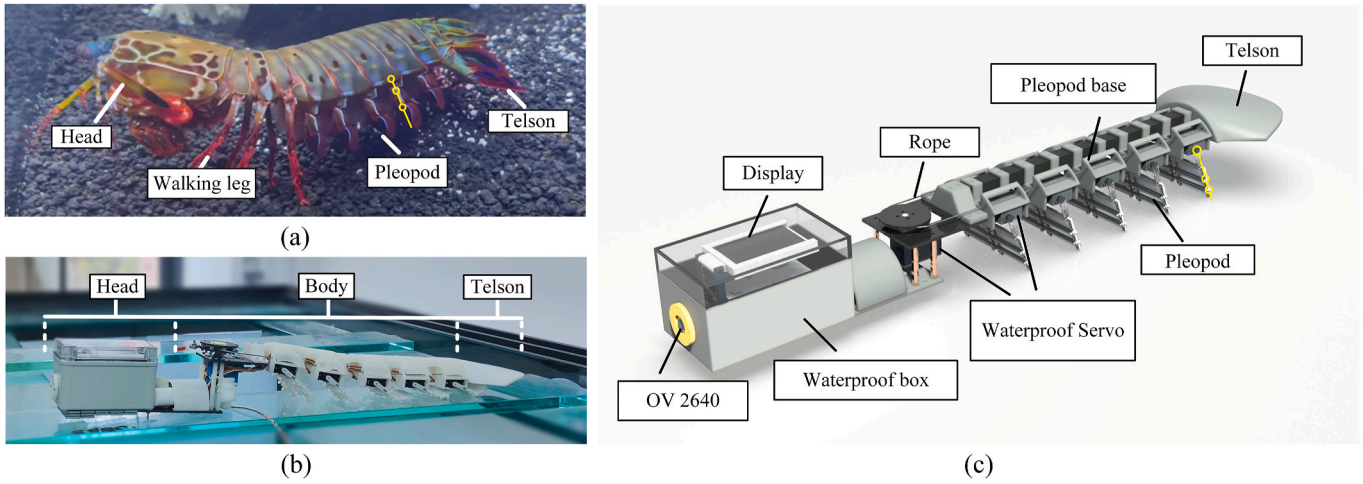

Fig. 1. Biological mantis shrimp and bionic mantis shrimp robot. (a) Biological mantis shrimp (b) Bionic mantis shrimp robot (c) Bionic mantis shrimp robot model.

robots that faithfully simulate the swimming capabilities of mantis shrimp. Therefore, the development of a bionic mantis shrimp robot with outstanding performance represents a meaningful endeavor based on the study of mantis shrimp movement.

An underwater robot with exceptional motion capabilities forms the foundation for successfully executing target tracking tasks. Additionally, the robot must gather external information through various sensors to accomplish underwater target tracking (Cong et al., 2021). Cameras, due to their cost effectiveness and ability to capture rich information, have gained widespread use in this context. For instance, Sun et al. implemented target tracking of robotic fish using embedded vision systems (Sun et al., 2013), while Yan et al. achieved autonomous underwater vehicle recovery through camera-based assessment of L-shaped optical arrays (Yan et al., 2019). It is evident that robots equipped with cameras for underwater target characterization play a pivotal role in tasks such as target tracking, localization, and navigation, presenting significant opportunities for application.

The accomplishment of the autonomous target tracking task by a robot hinges on its precise motion control. Central pattern generators (CPGs) represent a natural mechanism employed by animals to generate rhythmic motion control signals (Hjalmarsson, 2005). This mechanism has found extensive utility in governing the motion of bionic robots (Kiehn and Butt, 2003; Yu et al., 2014). The CPG controller allows for the adjustment of rhythmic robot motion with minimal parameters, resulting in efficient and stable motion control (Ijspeert, 2008). Achieving closed-loop control of the robot is primary to enabling it to sense its surroundings and adapt accordingly. Closed-loop CPG control stands as an effective approach to enhancing propulsion efficiency and maneuverability in robots.

For instance, in the work of Chen et al. a robot fish successfully avoided obstacles and followed a predetermined direction by employing closed-loop CPG control (Chen et al., 2021). Similarly, Wang et al. devised a motion controller for a bionic boxfish robot based on CPG, validating the effectiveness and stability of both open-loop and closed-loop CPG controllers through experimental trials (Wang and Xie, 2014). Korkmaz et al. combined CPG with fuzzy control to effectively govern the movement of robotic fish (Korkmaz et al., 2021). These studies collectively demonstrate that a CPG-based closed-loop control system can aptly sense the external environment and adjust the robot's motion state.

However, it is noteworthy that the closed-loop CPG control studied thus far has been primarily centered on single-joint or multijoint designs, with no prior exploration of closed-loop CPG control for robots with multiple pleopods engaged in coupled motion. Consequently, there is significant merit in devising a closed-loop CPG control system tailored to multipleopod coupled motion.

The contributions presented in this paper can be summarized as follows:

1. Leveraging insights from the physiological structure and motion mechanisms of the mantis shrimp, we designed a bionic mantis shrimp robot for underwater detection in narrow environments. The hardware system design of this robot has been fully realized. The robot's design incorporates rigid-flexible coupling, facilitating flexible underwater movement.
2. We have established a biomimetic closed-loop CPG control system based on the coordinated motion of multiple pleopods. This control system integrates CPG control, proportional integral derivative (PID) control, and fuzzy logic control (FL) to dynamically adjust the robot's movement direction and velocity based on the analysis of data collected by the visual sensor. This enables the robot to effectively track specific targets.
3. The flexibility of movement exhibited by the bionic mantis shrimp robot and the efficacy of the bionic closed-loop CPG control system have been validated through experimental trials involving the tracking of static and dynamic targets. This validation lays a solid foundation for the potential underwater applications of the bionic mantis shrimp robot.

The subsequent sections of this paper are structured as follows: Section 2 describes the biological mantis shrimp structure and introduces the design of our bionic mantis shrimp robot. Section 3 provides a comprehensive overview of the closed-loop CPG-based control system's design. Section 4 details the experiments conducted to assess the swimming performance of the bionic mantis shrimp robot in static and dynamic target tracking scenarios, thereby affirming the control system's effectiveness. Finally, Section 5 presents a concise discussion and conclusion.

2. Design of the bionic mantis shrimp robot

The development of a bionic mantis shrimp robot includes two key components: the mechanical structure system and the control hardware system. The mechanical structure system is rigorously designed to align with the motion characteristics of the biological mantis shrimp, ensuring its optimization for underwater operational scenarios. Meanwhile, the control hardware system plays a pivotal role in executing visual detection and motion control tasks, enabling the robot to promptly react to feedback from environmental information and thereby achieve autonomous control.

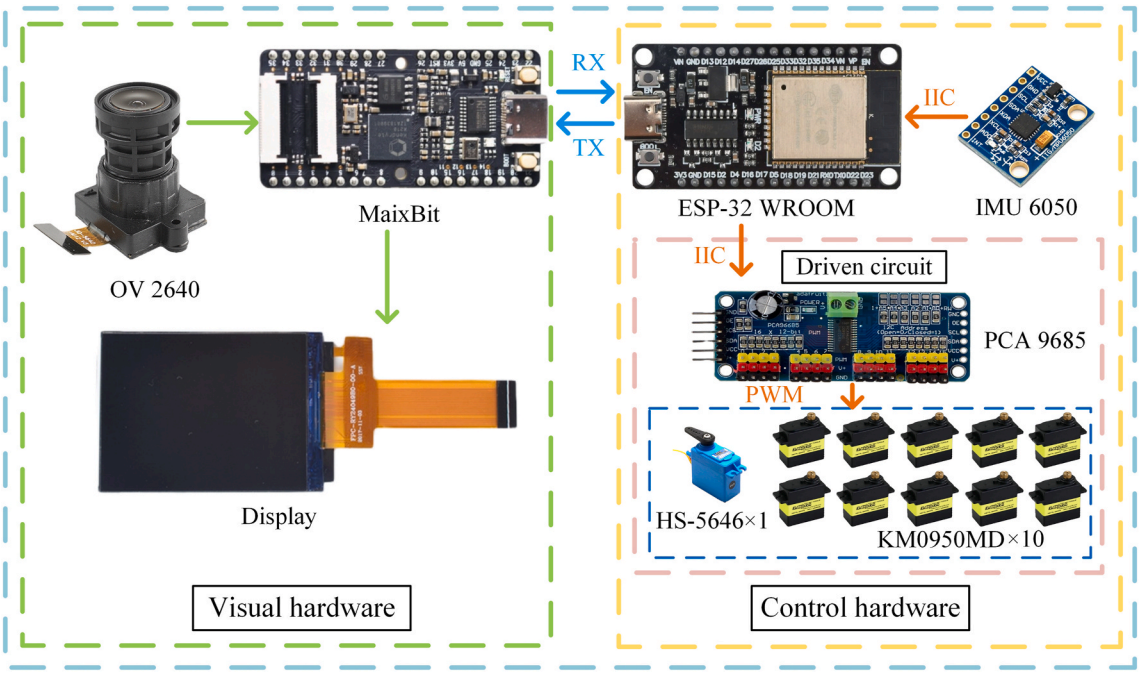

Fig. 2. Control hardware system.

2.1. *Mechanical structure system*

Fig. 1 illustrates the mechanical structure designed to replicate the motion of a mantis shrimp, enabling efficient and flexible underwater movement. As depicted in Fig. 1(a), our bionic mantis shrimp comprises distinct components, including the head, body, walking legs, pleopods, and telson. Among these elements, the five pairs of pleopods situated on the body serve as the primary source of propulsion. Fig. 1(b) and (c) present an overview of the robot's overall structure and highlight crucial components. Notably, a waterproof enclosure is affixed to the robot's head to house the control hardware. This enclosure is constructed from acrylonitrile butadiene styrene plastic, a thermoplastic renowned for its favorable comprehensive properties. On the body of the robot, five pleopod bases are strategically positioned, with two waterproof servomotors mounted on each pleopod base to govern the movement of a corresponding pair of pleopods. The robot generates its swimming thrust in water through the reciprocal paddling motion of the five pairs of pleopods located on both sides of the body. To effect turning maneuvers, the robot employs a flexible spine actuated by wire rope mechanisms. The predominant material employed in robot construction is photosensitive resin produced via 3D printing. This choice of material offers high molding precision and maintains stable physical properties when submerged underwater.

2.2. *Control hardware system*

Fig. 2 provides an overview of the control system utilized in our bionic mantis shrimp robot, which is divided into two primary components: the vision hardware and the motion control hardware. The vision hardware comprises the OV2640 camera, Liquid Crystal Display, and the MaixBit vision control board. This subsystem is tasked with processing image data and performing operations such as denoising, correction, color filtering, binarization, and anchor frame annotation. Subsequently, the processed image, which includes critical information such as object center coordinates and distance, is transmitted to ESP32 for further processing. The control hardware primarily includes the ESP-32-WROOM, inertial measurement unit (IMU6050), PCA 9685 servo drive board, and waterproof servomotors. This hardware component is responsible for regulating motion parameters through logical operations, thereby facilitating comprehensive motion control of the robot.

As depicted in the driving circuit illustrated in Fig. 2, the motion control of our bionic mantis shrimp robot necessitates the use of 11 servomotors. Among these, 10 servomotors are dedicated to governing the motion of the five pairs of pleopods, while one servomotor oversees the robot's turning motion. The PCA 9685 servo drive board, which is capable of driving 16 servos through IIC communication, aligns perfectly with the control requirements. The motion control board, ESP-32-WROOM, possesses the capability for dual-threaded operation. This dual-threaded functionality enables simultaneous execution of motion control signal output and processing of environmental feedback information. This approach leverages the full spectrum of available hardware resources, enabling the vision hardware system and the motion control system to function independently. This design choice also facilitates the incorporation of hardware upgrades in the future.

3. Closed-loop CPG-based target tracking control method

3.1. *CPG motion control*

CPGs play a pivotal role in orchestrating rhythmic motion in vertebrates. Building upon the Ijspeert oscillator and taking into account the distinctive features of the mantis shrimp's abdominal foot movement (Ijspeert et al., 2007; Crespi et al., 2008), along with the associated gait equation, we introduce a CPG oscillator model tailored to the mantis shrimp robot:

$$\dot{\theta}_i = \omega_i + \sum_j h_{1j} w_{ij} \sin\left(\theta_j - \theta_i - \varphi_{ij}\right) \tag{1}$$

$$\ddot{h}_{1i} = \alpha_i \left(\frac{\alpha_i}{4} \left(H_{1i} - h_{1i} \right) - \dot{h}_{1i} \right) \tag{2}$$

$$\ddot{h}_{2i} = \alpha_i \left(\frac{\alpha_i}{4} \left(H_{2i} - h_{2i} \right) - \dot{h}_{2i} \right) \tag{3}$$

$$\ddot{x}_i = \alpha_i \left(\frac{\alpha_i}{4} \left(X_i - x_i \right) - \dot{x}_i \right) \tag{4}$$

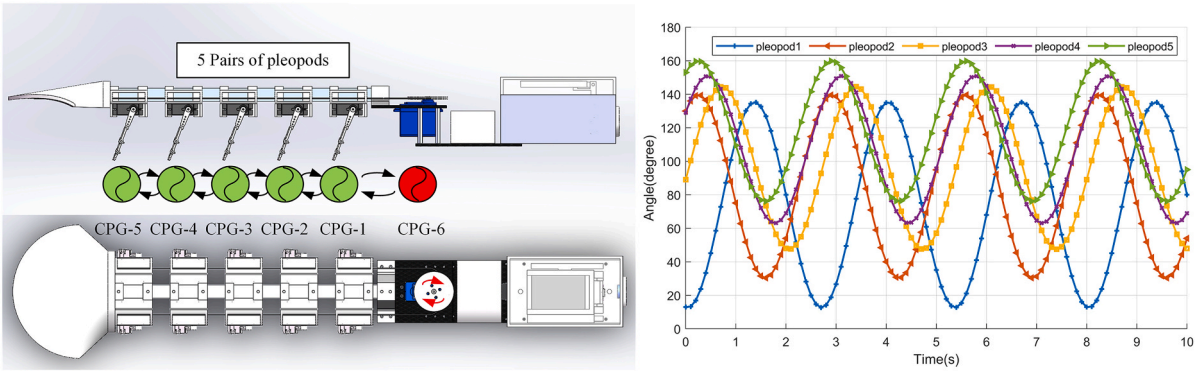

Fig. 3. CPG motion controller of the bionic mantis shrimp robot (a) Topology of the CPG network (b) CPG motion control simulation of pleopods.

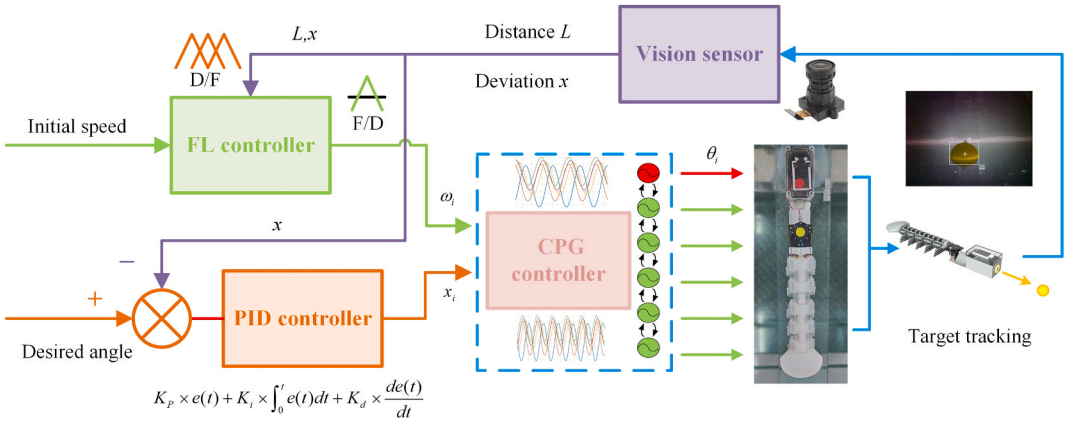

Fig. 4. Block diagram of CPG-based closed-loop control for target tracking.

$$\beta_i = x_i + \sqrt{h_{1i}^2 + h_{2i}^2}\sin(\theta + \gamma) \tag{5}$$

$$\tan\gamma = \frac{h_{1i}}{h_{2i}} \tag{6}$$

where ω_i is the desired frequency of the oscillator. θ_i represents the output phase state variable of the ith oscillator. x_i, h_{2i}, and h_{1i} represent the output deviation term and amplitude state variable in the oscillator i. α_i is constant positive gains. w_{ij} and φ_{ij} are parameters respectively coupling weights and phase biases which determine how oscillator j influences oscillator i. H_{1i}, H_{2i}, and X_i are parameters of controller representing the desired amplitude of each corresponding output term of the oscillator. β_i represents the final output angle of each oscillator.

We amalgamate the output of this oscillator with the motion gait of the bionic mantis shrimp robot. This integration allows for the facile adjustment of multiple amplitude parameters, as well as the frequency and phase differences associated with each oscillator, in accordance with the specific motion requirements. Consequently, the robot's motion can be flexibly controlled.

In Fig. 3(a), the topology of a CPG network is depicted, demonstrating the coupled motion of multiple pleopods. This CPG network includes six oscillators, which include a central oscillator governing the robot's turning motion and additional oscillators responsible for regulating the coupled motion of the five pairs of pleopods. Fig. 3(b) exhibits the simulated output signals of the oscillator controlling pleopod motion. It is evident that each pair of pleopods exhibits distinct motion angles and amplitudes at various instances.

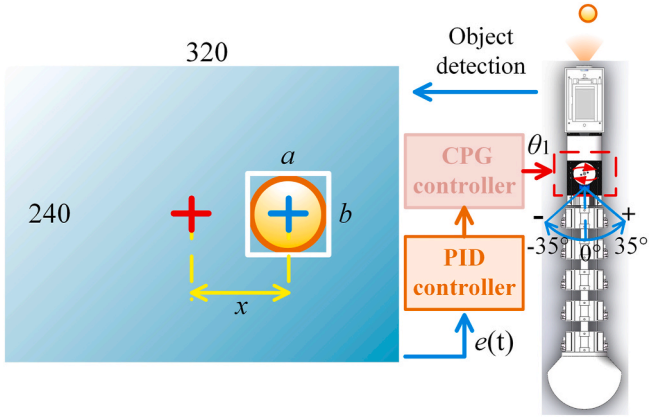

Fig. 5. Principle diagram of closed-loop direction control.

3.2. CPG-based closed-loop control of target tracking

The CPG-based closed-loop control approach proposed in this study includes two essential components: direction control and velocity control, each responsible for adjusting the tracking motion's direction and velocity, respectively. These components collaborate harmoniously to achieve precise tracking of the target. Fig. 4 illustrates the control block diagram of the system, wherein the CPG-based closed-loop controller comprises three integral elements: the CPG controller, PID controller, and FL controller.

The CPG controller primarily governs the robot's motion, while the PID controller modulates the output of the central oscillator to effect direction closed-loop control. Concurrently, the FL controller fine-tunes

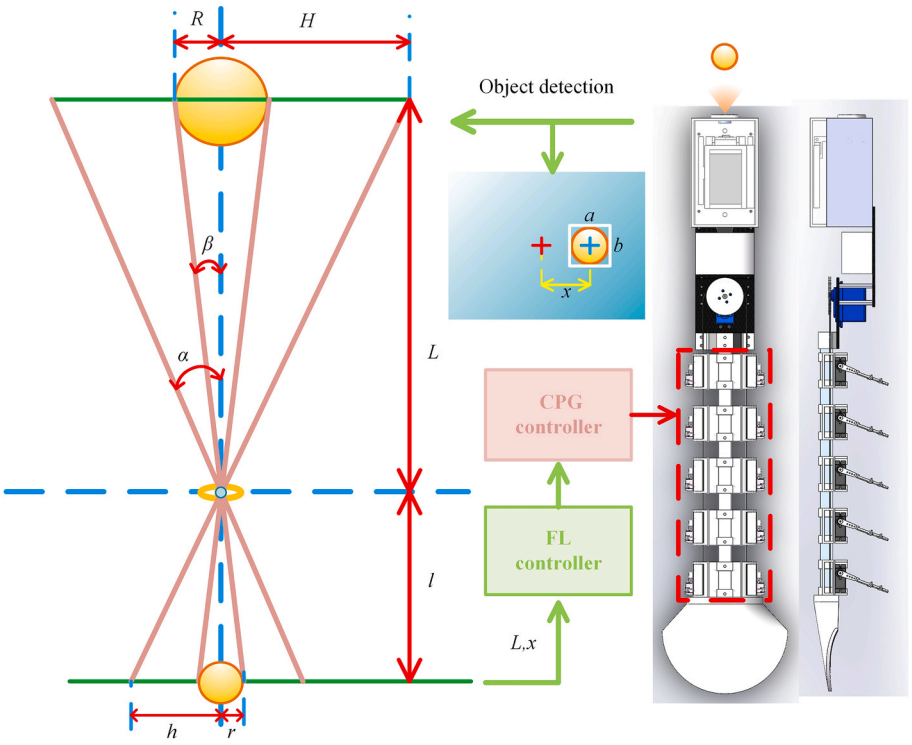

Fig. 6. Principal diagram of closed-loop velocity control.

the pleopod oscillator's output to regulate the robot's tracking velocity.

The overarching workflow unfolds as follows: Visual sensor data capture target information, which is subsequently transmitted to the visual control board. Following processing, the visual feedback information is conveyed to the motion controller via the serial port. The motion controller evaluates the horizontal deviation detected in the visual information through the PID controller, thus adjusting the CPG parameters to facilitate robot turning control. For robot velocity control, the FL controller takes into account both the horizontal deviation and distance information from the visual data to adapt the CPG oscillation frequency, thereby accomplishing robot velocity control. Together, these components collaborate seamlessly to achieve precise adjustments in the robot's motion direction and velocity, ultimately resulting in accurate tracking of the target object.

3.2.1. *Closed-loop direction control*

Fig. 5 elucidates the underlying principle of closed-loop direction control. It involves the detection of the deviation between the robot's actual position and the target position, which is subsequently employed to fine-tune the robot's motion direction. The closed-loop direction control for the bionic mantis shrimp robot is realized through the utilization of a PID controller for adjusting the CPG parameter controller. As depicted in Fig. 5, the dimensions of the image acquired from the vision sensor measure 320 × 240 pixels. The length and width of an anchor frame are a and b respectively. The distance between the center of the rectangular frame and the center of the image is x. The input deviation signal $e(t)$ of the PID controller is calculated as:

$$e(t) = x - x(t) \tag{7}$$

One of the input parameters of the CPG model D(t) is obtained through the PID controller with the following expression:

$$D(t) = K_P \times e(t) + K_i \times \int_0^t e(t)dt + K_d \times \frac{de(t)}{dt} \tag{8}$$

$$D(t) = \begin{cases} 35^\circ, D(t) > 35^\circ \\ D(t), -35^\circ \le D(t) \le 35^\circ \\ -35^\circ, D(t) < -35^\circ \end{cases} \tag{9}$$

where D(t) is the offset of the CPG model, which is the only change parameter when the bionic mantis shrimp robot adjusts its motion direction. $e(t)$ is the error of the input. K_p, K_i, and K_d are the proportional, integral and differential coefficients of the PID controller, respectively.

Several underwater tests were conducted to assess the turning performance of our bionic mantis shrimp robot while employing different PID parameters. Based on the results and subsequent analysis, we opted for a proportional-integral control strategy to enhance the robot's turning performance. Specifically, the values of K_p, K_i, and K_d were set to 0.7, 0.2 and 0, respectively. It is crucial to note that the range of D(t), denoting the turning angle, has been constrained within [−35°, 35°] to ensure the structural integrity of the robot. In practice, the bionic mantis shrimp robot dynamically adjusts its motion direction based on the error, represented as e(t), to effectively track the target and maintain stable swimming behavior.

3.2.2. *Closed-loop velocity control*

Fig. 6 illustrates the fundamental concept of closed-loop velocity control. The robot effectively sustains an appropriate tracking velocity by first detecting the horizontal deviation and distance from the target object and then adjusting its motion velocity in accordance with predefined fuzzy rules. This closed-loop velocity control relies on the target information acquired by the vision sensor. As depicted in Fig. 6, the actual physical world is situated above the blue dashed line, while the camera's perspective of the world is below this line. Leveraging the geometric relationship between these perspectives, we can derive the following relationship:

$$\tan\alpha = \frac{h}{l} \tag{10}$$

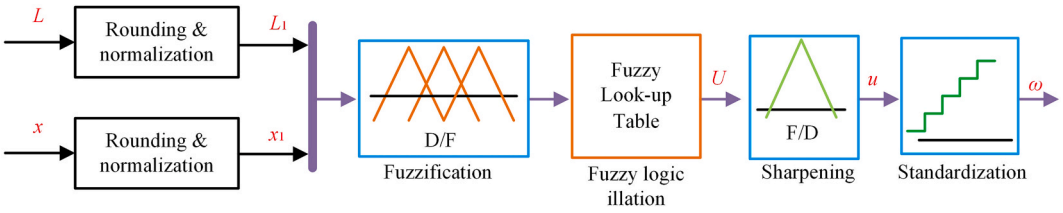

Fig. 7. Fuzzy logic controller.

Table I
Fuzzy rule table.

Frequency ω		Distance L		
		SD	MD	LD
Deviation x	SX	S	L	VL
	MX	VS	M	VL
	LX	VS	M	L

$$\tan\beta = \frac{r}{l} = \frac{R}{L} \tag{11}$$

By combining the equation:

$$L = \frac{R \cdot h}{r \cdot \tan\alpha} \tag{12}$$

$$r = \frac{a+b}{4} \tag{13}$$

where L is the distance between the robot and the target object, R is the

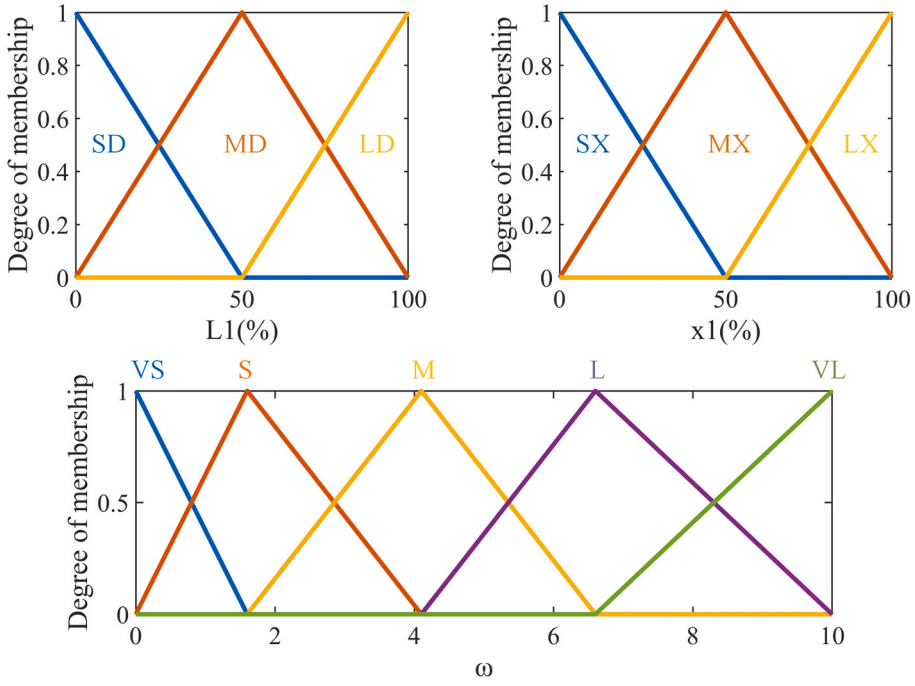

Fig. 8. Affiliation functions L_1, x_1, ω

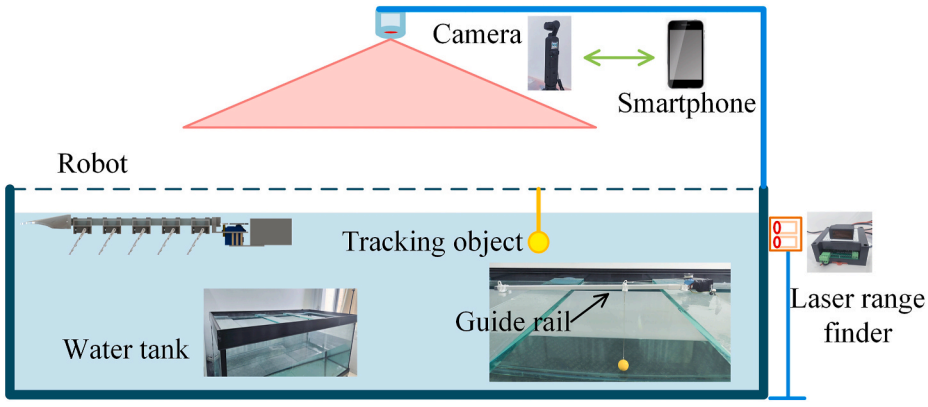

Fig. 9. Experimental platform and equipment.

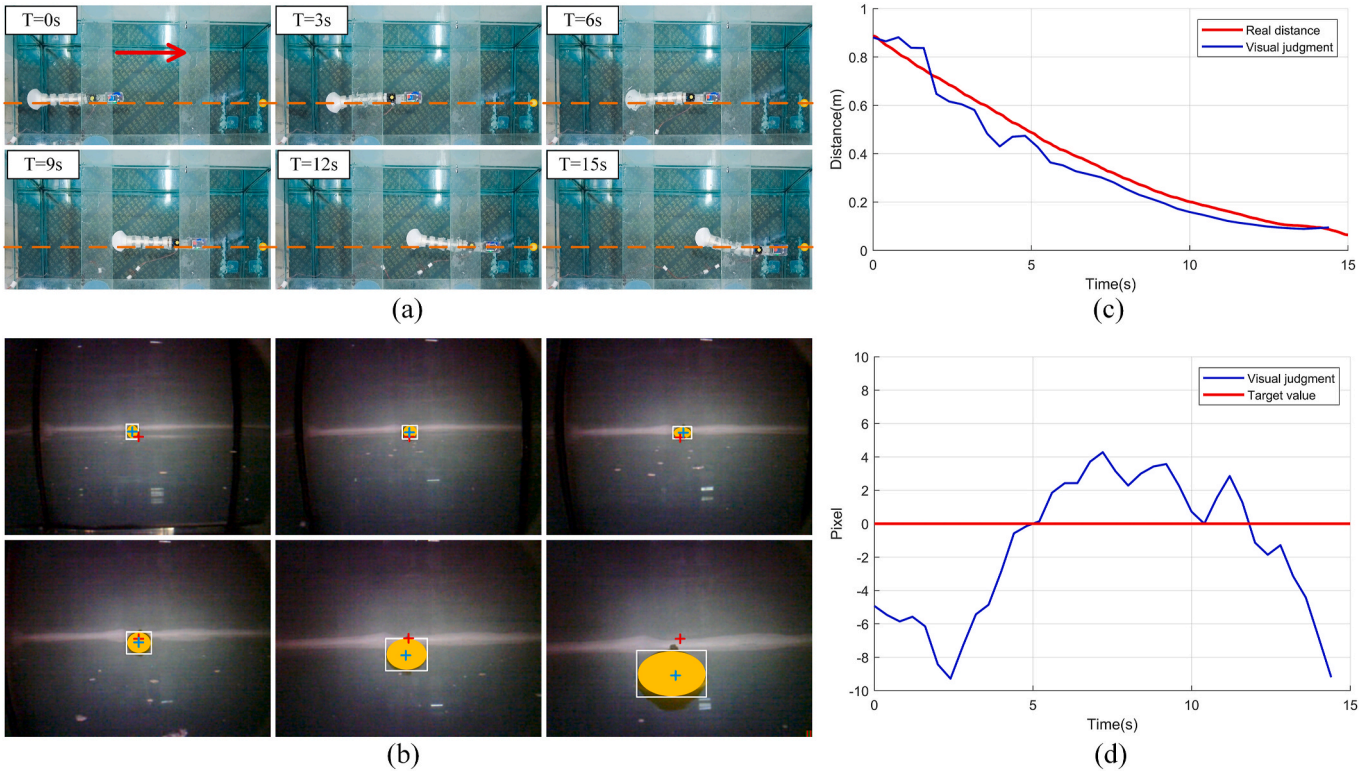

Fig. 10. Robot static target tracking experiment. (a) Time series plot of robot motion. (b) Target detection plot recorded from the first view of the robot. (c) Comparison of visual judgment distance and real distance. (d) Deviation of the object in the horizontal direction of the visual field.

true radius of the target object, r is the pixel occupied by the radius of the target object in the vision sensor, and l is the image distance. h is a fixed pixel value, and α is half of the vision sensor field of view.

Fig. 7 presents the autonomous velocity control mechanism designed using an FL controller. To optimize hardware resource utilization and enhance motion stability in the bionic mantis shrimp robot, a Mamdani-type inference approach, triangular membership functions, and centroid defuzzification are employed.

Table I outlines the fuzzy rules governing the FL controller, as determined through experimentation. These rules are responsible for setting the motion frequency ω of the pleopods based on two key parameters: distance (L) and horizontal deviation (x). Distance (L) is categorized into three levels, ranging from near to far: SD, MD, and LD. The deviation x is divided into three levels from small to large: SX, MX, and LX. The movement frequency is divided into five levels from slow to fast: VS, S, M, L, and VL. Fig. 8 illustrates the membership functions for distance (L), deviation (x), and motion frequency (ω). It is worth noting that due to potential variations in the size of anchor frames, often influenced by lighting conditions, during target object detection with the visual sensor, a normalization step is applied to the defuzzified output. This normalization ensures that the output corresponds to a reasonable motion frequency, contributing to the robot's stable tracking performance.

4. Experiments

Fig. 9 illustrates the experimental platform utilized to validate the efficacy of the CPG-based target tracking closed-loop control system. The experimental pool measures 2 m × 1 m × 1 m in size and is equipped with a camera positioned atop the pool. Within this setup, a yellow ball, serving as the target, can traverse along a guide rail. The robot's swimming activities are captured by the camera, which interfaces with a smartphone for real-time observation of the robot's movements. To record the robot's tracking motion, the robot employs the body vision control board to capture its initial perspective. Additionally, a laser range finder is employed to externally measure variations in the robot's distance traveled. The motion state of the robot is deduced by processing the time-series data representing its swimming behavior.

4.1. Static target tracking

As depicted in Fig. 10, the bionic mantis shrimp robot demonstrates its ability to track a stationary target object in a straight-line trajectory. The target object remains fixed in front of the robot as it initiates motion from a stationary position. Fig. 10(a) exhibits a series of time-series diagrams depicting the robot's motion. Notably, it is evident that the robot swiftly approaches the target object within the 0–6 s interval, decelerating between 9 and 15 s when in closer proximity to the target. This behavior aligns with the predefined control rules. The relative position of the orange baseline and the robot within the figure substantiates the robot's capacity to maintain straight-line tracking effectively.

Fig. 10(b) presents an image captured by the robot's first-person perspective during target object detection. In this image, the red cross represents the center of the field of view, the white box encloses the target object, the blue cross marks the center of the target object, and the control target is defined as the intersection of the two crosses.

Fig. 10(c) illustrates a comparison between the distance of the target object as determined by the robot and the actual distance. While both trajectories exhibit similar trends, a slight discrepancy exists, with a maximum error of 0.13 m observed at 4 s. It is important to note that target object recognition relies on color filtering, rendering it sensitive to variations in lighting conditions. Consequently, complex underwater lighting can influence the accuracy of target object localization.

Fig. 10(d) portrays changes in the target object's horizontal offset within the visual field during the robot's motion. In this depiction, positive pixel values indicate that the target object resides on the right side of the robot, while negative pixel values signify the target object's

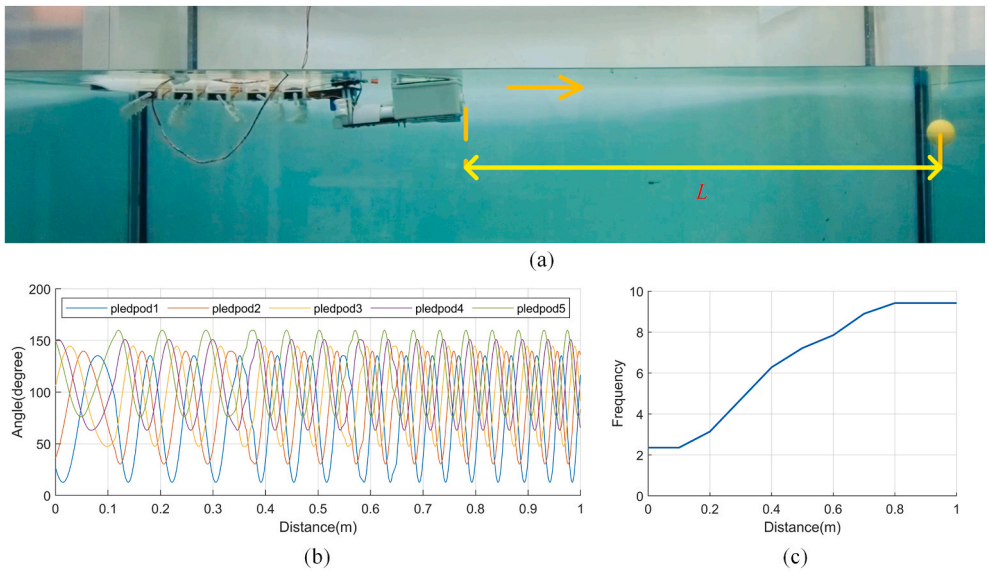

Fig. 11. Robot static target tracking experiment (a) Side view of robot motion (b) CPG controller output variation (c) Output frequency variation of CPG controller.

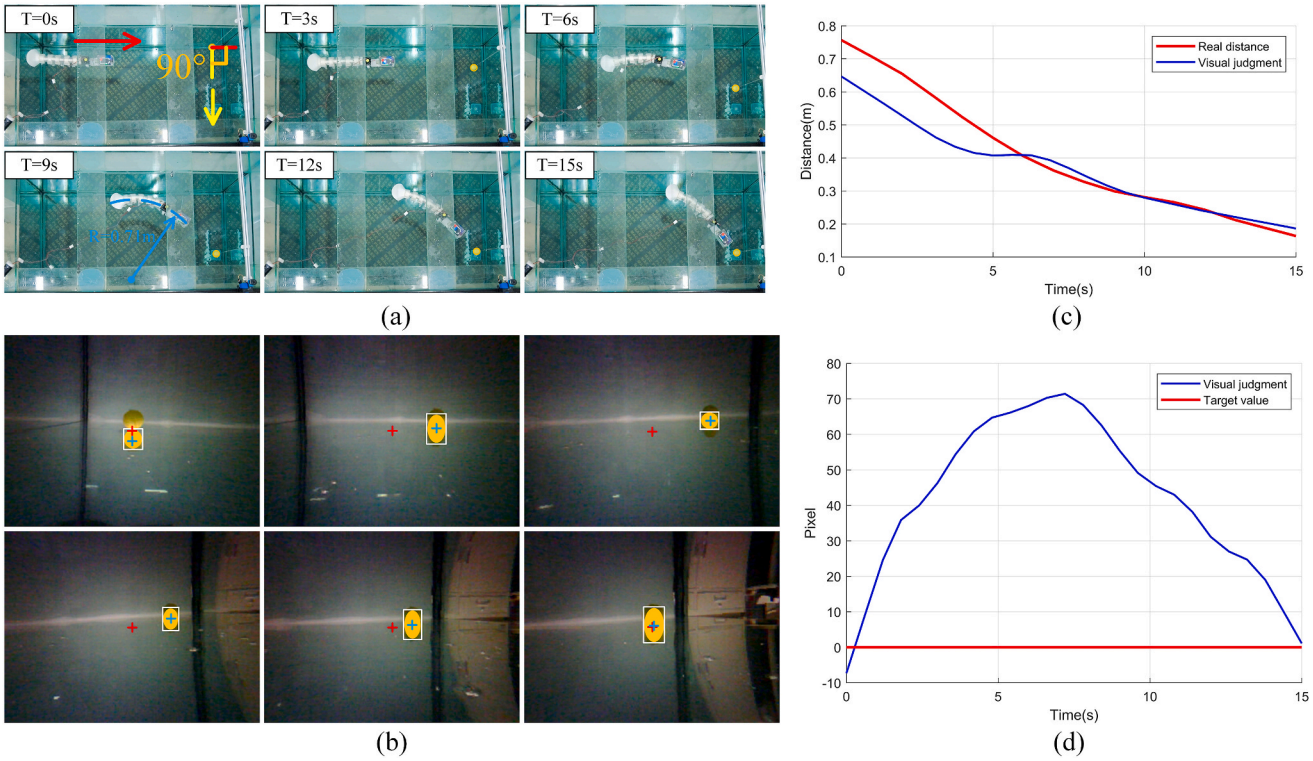

Fig. 12. Robot dynamic target tracking experiment (a) Time series of robot motion (b) Target detection diagram recorded from the first view of the robot (c) Comparison of visual judgment distance and real distance (d) Deviation of the target in the horizontal direction of the visual field.

location on the left side of the robot. The robot continually adjusts its tracking direction during motion, maintaining a left-right deviation within 11 pixels. This observation underscores the robot's overall tracking stability, with minimal directional fluctuations.

Fig. 11 presents the output angle of the pleopod CPG model, while the bionic mantis shrimp robot engages in straight-line tracking of a stationary target object. Notably, the motion frequency of the pleopod varies in accordance with the distance L from the target. It becomes evident that as the robot moves farther away from the target, the oscillation frequency of the CPG model - and consequently, the pleopod's paddling frequency - increases. Conversely, as the robot progressively approaches the distance to the target, the pleopod's motion frequency decelerates. The oscillation frequency ranges from a maximum of 3π to a minimum of $3/4\pi$, aligning precisely with the established velocity closed-loop control rule.

4.2. *Dynamic target tracking*

Fig. 12 provides insight into the experimental process and results of the bionic mantis shrimp robot as it tracks a dynamic target. The target, following a constant velocity of 0.1 m/s in alignment with the direction indicated by the yellow arrow, ceases movement upon reaching its limit

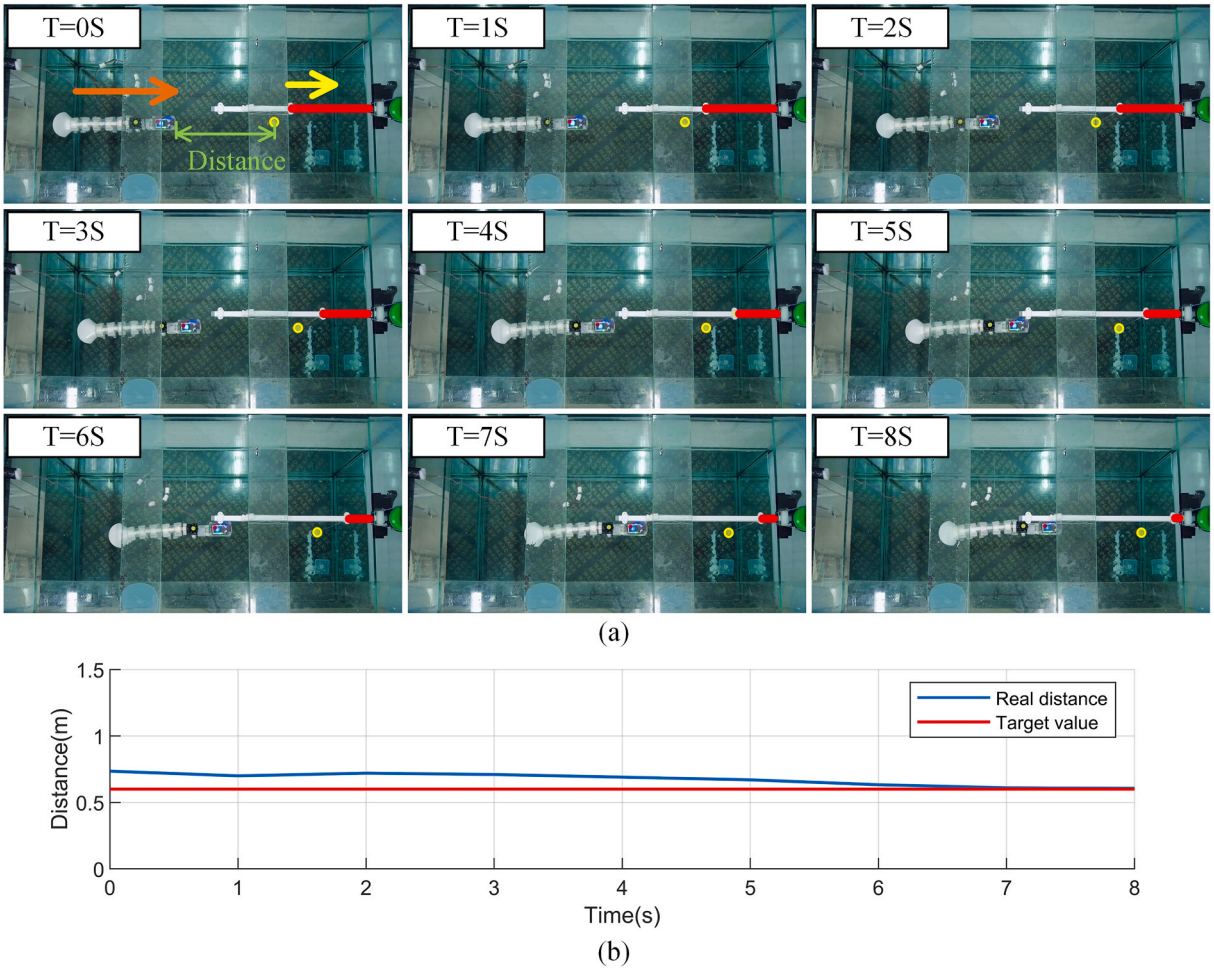

Fig. 13. Experiment of the robot tracking a target object moving in the same direction. (a) Time series diagram of robot motion. (b) Real distance and target value.

position. The robot commences from a stationary position perpendicular to the direction of the target's motion.

Fig. 12(a) illustrates the time-series data capturing the robot's motion. It is evident that the robot adeptly follows the target object, continuously adjusting its orientation in real time, ultimately achieving smooth tracking after approximately 13 s.

In Fig. 12(b), the time-series data portrays the changes within the robot's field of view from its first-person perspective.

Fig. 12(c) offers a comparison between the robot's perceived distance to the target and the actual distance. Notably, when the distance between the robot and the target exceeds 0.4 m, the distance estimation is less accurate. In contrast, when the distance is relatively close, the actual and estimated distances closely align. This discrepancy primarily arises from the proximity of the target to the water's surface, resulting in reflections within the water. Additionally, fluctuations in lighting conditions as the target changes position can lead to enlarged anchor frames, contributing to less precise distance estimations.

Fig. 12(d) portrays variations in the target's horizontal offset during the robot's motion. Due to the rapid lateral motion of the target, the horizontal deviation increases swiftly, reaching a maximum deviation of 71 pixels at 7 s. However, with the target reaching its limit position and the robot adjusting its turning angle, the robot effectively realigns the target to the center of its field of view, accomplishing this correction within approximately 5 s of motion adjustment.

Tracking experiments were undertaken to further substantiate the target tracking capabilities of the bionic mantis shrimp robot. Fig. 13 depicts the robot successfully tracking a target object that is moving in the same direction. The target initiates motion at a velocity of 0.15 m/s, while the robot commences from a state of rest and follows the target by continuously gauging the distance between them and adjusting its own velocity accordingly. Remarkably, the robot consistently maintains a distance exceeding 0.6 m from the target within an 8 s timeframe. This achievement is attributed to the robot's velocity adjustments, in accordance with the established fuzzy rule, which align closely with the target's running velocity. It is evident that dynamic targets with specific velocities can be effectively tracked within a defined distance range.

Fig. 14 demonstrates the robot's tracking performance when pursuing a horizontally moving target object. The target object initiates motion at a velocity of 0.1 m/s, while the robot traverses the pool diagonally, forming an angle of 130° between its velocity direction and that of the target. Upon detecting the target, the robot promptly adjusts its orientation and continuously adapts the bending angle of its torso in response to the target's motion. The radius of the turning movement varies from 1.4 m to 0.65 m. Remarkably, the robot effectively narrows the distance to the target following a brief period of substantial turning, ultimately achieving target tracking after 14 s of continuous adjustments. This observation underscores the feasibility of the bionic mantis shrimp robot's movement tracking capabilities within confined underwater spaces.

Table II consolidates data from both static tracking experiments and dynamic tracking experiments. The robot exhibits an average distance judgment error of 0.13 m during motion. This discrepancy primarily arises from the monocular distance measurement method relying on color recognition, which is notably influenced by underwater lighting conditions. Consequently, color filtering introduces substantial noise, thereby impacting the accuracy of the anchor box.

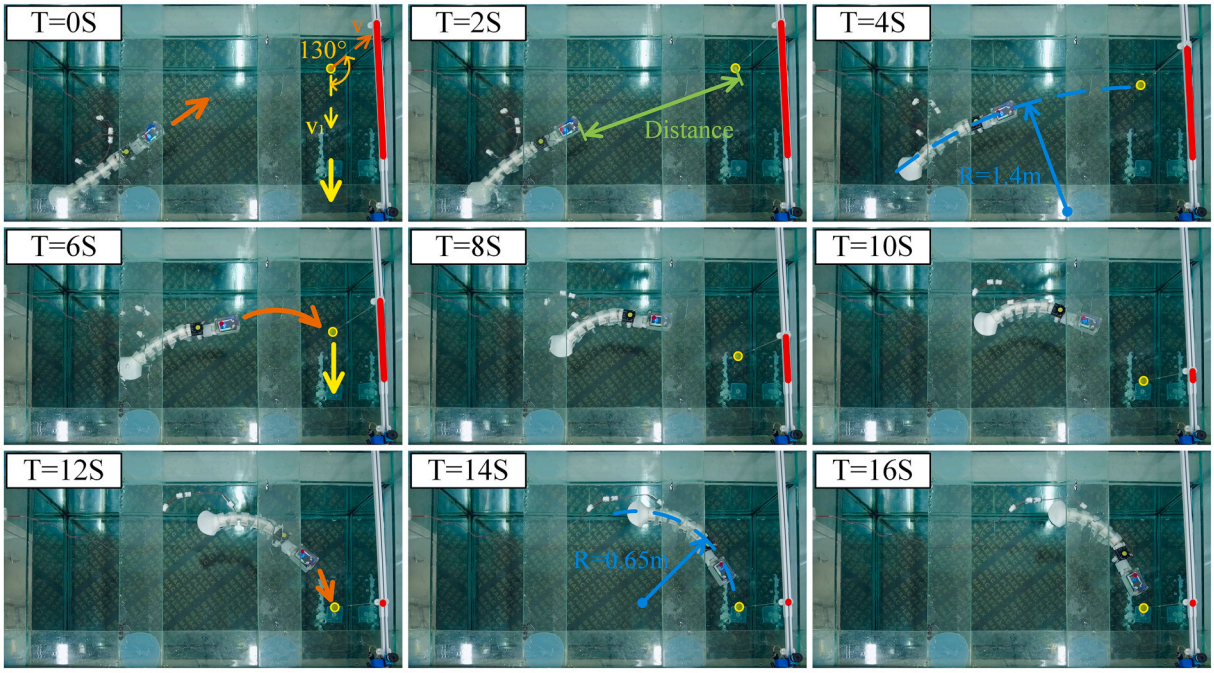

(a)

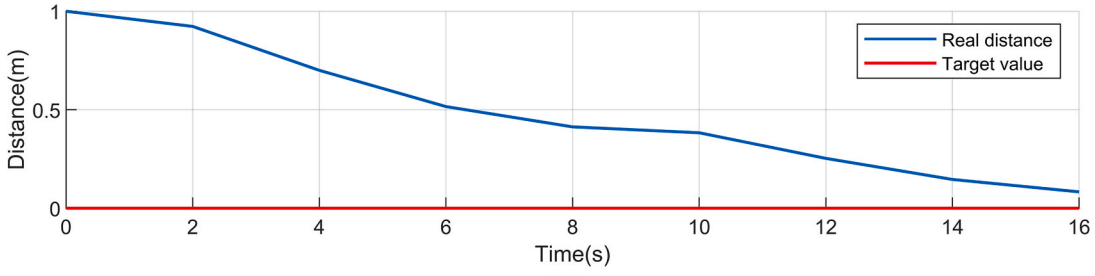

(b)

Fig. 14. Large-angle dynamic tracking experiment of the robot. (a) Time series diagram of robot motion (b) Real distance and target value.

Table 2
Experimental results.

Type of experiment	The velocity of the target	The angle of motion with the target	Maximum distance error	Maximum deviation	Minimum turning radius
Static straight tracking	0 m/s	0°	0.13 m	11 Pixel	/
Dynamic tracking I	0.1 m/s	90°	0.12 m	72 Pixel	0.71 m
Dynamic tracking II	0.1 m/s	130°	0.14 m	46 Pixel	0.65 m

In scenarios involving target objects with varying motion angles relative to the robot, the robot demonstrates real-time motion adjustments to ensure that the target object remains centered within its field of view. Furthermore, the robot maintains a minimum turning radius within 1 m, coinciding with the width of the experimental pool (1 m). The experiments affirm that the bionic mantis shrimp robot, driven by bionic closed-loop CPG control, effectively accomplishes the task of tracking specific targets.

5. Conclusion and future work

This paper adopts the mantis shrimp as a bionic model, leading to the design of the bionic mantis shrimp robot and its accompanying hardware system. Furthermore, it introduces a closed-loop CPG-based target tracking control system. Conclusive insights emerge from the robot's tracking experiments involving both static and dynamic targets. The designed bionic mantis shrimp robot in this paper exhibits the capability to swiftly adapt its tracking velocity and direction in response to horizontal deviation and target distance. It effectively accomplishes target tracking tasks even when confronted with obtuse angles (e.g., 130°) between the robot's motion direction and that of the target. Impressively, it achieves a minimal tracking turning radius of 0.65 m. Moreover, the robot demonstrates the capacity to track dynamic targets with a velocity of 0.15 m/s within a defined distance range. However, it is important to acknowledge that the robot's motion control algorithm presently exhibits only moderate robustness, partly due to hardware limitations. Additionally, the reliance on color filtering for target recognition restricts the robot's recognition and tracking capabilities in complex environments.

Future work will involve the integration of optimization algorithms in conjunction with hydrodynamic analyses of the robot to enhance the efficiency and precision of controller parameter optimization. Hardware system enhancements, refinement of the robot's motion control algorithm, and the exploration of underwater perception algorithms based on multiple sensors will be pursued. These efforts aim to equip the bionic

mantis shrimp robot with the capacity to undertake tasks such as biological tracking, search and rescue, and obstacle avoidance in complex underwater environments.

CRediT authorship contribution statement

Gang Chen: Project administration, Writing – original draft, Writing – review & editing. **Yidong Xu:** Writing – original draft, Writing – review & editing, Validation. **Xin Yang:** Data curation, Formal analysis. **Huosheng Hu:** Writing – review & editing. **Hao Cheng:** Software. **Lvyuan Zhu:** Supervision. **Jingjing Zhang:** Visualization. **Jianwei Shi:** Software, Supervision. **Xinxue Chai:** Data curation.

Declaration of competing interest

The authors declare that they have no known competing financial interests or personal relationships that could have appeared to influence the work reported in this paper.

Data availability

Data will be made available on request.

Acknowledgements

This work was financially supported by National Natural Science Foundation of China (Nos. 52275037, 51875528 and 41506116), Zhejiang Provincial Natural Science Foundation of China (No. LR24E050002), the Key Research and Development Project of Zhejiang Province (Nos. 2023C03015 and 2021C04017), the Key Research and Development Project of Ningxia Hui Autonomous Region (No. 2023BDE03002), and Science Foundation of Zhejiang Sci-Tech University (ZSTU) (No. 17022183-Y).

References

Blair, S., Garcia, M., Davis, T., Zhu, Z., Liang, Z., Konopka, C., Kauffman, K., Colanceski, R., Ferati, I., Kondov, B., Stojanoski, S., Todorovska, M.B., Dimitrovska, N.T., Jakupi, N., Miladinova, D., Petrusevska, G., Kondov, G., Dobrucki, W.L., Nie, S., Gruev, V., 2021. Hexachromatic bioinspired camera for image-guided cancer surgery. Sci. Transl. Med. 13 https://doi.org/10.1126/scitranslmed.aaw7067.

Chen, Z., Um, T.I., Bart-Smith, H., 2012. Bio-inspired robotic manta ray powered by ionic polymer-metal composite artificial muscles. Int. J. Smart Nano Mater. 3, 296–308. https://doi.org/10.1080/19475411.2012.686458.

Chen, J., Yin, B., Wang, C., Xie, F., Du, R., Zhong, Y., 2021. Bioinspired closed-loop CPG-based control of a robot fish for obstacle avoidance and direction tracking. J. Bionic Eng. 18, 171–183. https://doi.org/10.1007/s42235-021-0008-0.

Chen, G., Lu, Y., Yang, X., Hu, H., 2022. Reinforcement learning control for the swimming motions of a Beaver-like, single-legged robot based on biological inspiration. Robot. Auton. Syst. 154, 1–12.

Chen, G., Xu, Y., Yang, C., Yang, X., Hu, H., Chai, X., Wang, D., 2023a. Design and Control of a Novel Bionic Mantis Shrimp Robot. IEEE/ASME Transactions on Mechatronics 28, 3376–3385.

Chen, G., Yang, X., Xu, Y., Lu, Y., Huosheng, H., 2023b. Neural network-based motion modeling and control of water-actuated soft robotic fish. Smart Mater. Struct. 32, 015004.

Chen, G., Peng, W., Wang, Z., Tu, J., Hu, H., Wang, D., Cheng, H., Zhu, L., 2023c. Modeling of swimming posture dynamics for a beaver-like robot. Ocean Eng 279, 114550.

Cong, Y., Gu, C., Zhang, T., Gao, Y., 2021. Underwater robot sensing technology: a survey. Fundamental Research 1, 337–345. https://doi.org/10.1016/j.fmre.2021.03.002.

Crespi, A., Lachat, D., Pasquier, A., Ijspeert, A.J., 2008. Controlling swimming and crawling in a fish robot using a central pattern generator. Aut. Robots 25, 3–13.

Garayev, K., Murphy, D.W., 2021. Metachronal swimming of Mantis shrimp: kinematics and interpleopod vortex interactions. Integr. Comp. Biol. 61, 1631–1643. https://doi.org/10.1093/icb/icab052.

Hjalmarsson, H., 2005. From experiment design to closed-loop control. Automatica 41, 393–438. https://doi.org/10.1016/j.automatica.2004.11.021.

Ijspeert, A.J., 2008. Central pattern generators for locomotion control in animals and robots: a review. Neural Network. 21, 642–653. https://doi.org/10.1016/j.neunet.2008.03.014.

Ijspeert, A.J., Crespi, A., Ryczko, D., Cabelguen, J., 2007. From swimming to walking with a salamander robot driven by a spinal cord model. Science 315, 1416–1420.

Kiehn, O., Butt, S.J., 2003. Physiological, anatomical and genetic identification of CPG neurons in the developing mammalian spinal cord. Prog. Neurobiol. 70, 347–361. https://doi.org/10.1016/s0301-0082(03)00091-1.

Korkmaz, D., Ozmen Koca, G., Li, G., Bal, C., Ay, M., Akpolat, Z.H., 2021. Locomotion control of a biomimetic robotic fish based on closed loop sensory feedback CPG model. J. Mar. Eng. Technol. 20, 125–137. https://doi.org/10.1080/20464177.2019.1638703.

Li, X., Li, X., Hou, X., Li, Y., Meng, Y., Ma, L., Tian, Y., 2022. Mantis shrimp-inspired underwater striking device generates cavitation. J. Bionic Eng. 19, 1758–1770. https://doi.org/10.1007/s42235-022-00227-8.

Muralidharan, M., Palani, I.A., 2021. Development of subcarangiform bionic robotic fish propelled by shape memory alloy actuators. Defence Sci. J. 71, 94–101. https://doi.org/10.14429/dsj.71.15777.

Sun, F., Yu, J., Xu, D., Wang, M., 2013. Target Tracking of Robotic Fish Based on Embedded Vision and CPG Model. IEEE, pp. 1206–1211.

Wang, W., Xie, G., 2014. CPG-Based locomotion controller design for a boxfish-like robot. Int. J. Adv. Rob. Syst. 11, 87. https://doi.org/10.5772/58564.

Wang, G., Chen, X., Yang, S., Jia, P., Yan, X., Xie, J., 2017. Subsea crab bounding gait of leg-paddle hybrid driven shoal crablike robot. Mechatronics 48, 1–11. https://doi.org/10.1016/j.mechatronics.2017.10.002.

Yan, Z., Gong, P., Zhang, W., Li, Z., Teng, Y., 2019. Autonomous underwater vehicle vision guided docking experiments based on L-shaped light array. IEEE Access 7, 72567–72576. https://doi.org/10.1109/ACCESS.2019.2917791.

Yu, J., Tan, M., Chen, J., Zhang, J., 2014. A survey on CPG-inspired control models and system implementation. IEEE Transact. Neural Networks Learn. Syst. 25, 441–456. https://doi.org/10.1109/TNNLS.2013.2280596.

Yu, J., Wang, M., Dong, H., Zhang, Y., Wu, Z., 2018. Motion control and motion coordination of bionic robotic fish: a review. J. Bionic Eng. 15, 579–598. https://doi.org/10.1007/s42235-018-0048-2.